Heliyon 9 (2023) e17392

Contents lists available at ScienceDirect

Heliyon

journal homepage: www.cell.com/heliyon

Rev1 deficiency induces a metabolic shift in MEFs that can be manipulated by the NAD$^+$ precursor nicotinamide riboside

Sharath Anugula [a,1], Zhiquan Li [a,1], Yuan Li [a,1], Alexander Hendriksen [a], Peter Bjarn Christensen [a], Lin Wang [c], Jonathan M. Monk [c], Niels de Wind [b], Vilhelm A. Bohr [a,d], Claus Desler [a], Robert K. Naviaux [c], Lene Juel Rasmussen [a,*]

[a] *Center for Healthy Aging, Department of Cellular and Molecular Medicine, University of Copenhagen, DK-2200, Copenhagen, Denmark*
[b] *Department of Human Genetics, Leiden University Medical Center, Leiden, the Netherlands*
[c] *Departments of Medicine, Pediatrics, and Pathology, University of California, San Diego School of Medicine, 214 Dickinson Street, Building CTF, Room C107, San Diego, CA, 92103, USA*
[d] *Laboratory of Molecular Gerontology, National Institute on Aging, National Institutes of Health, Baltimore, MD, USA*

ARTICLE INFO

Keywords:
Rev1
Replication stress
NAD$^+$
Nicotinamide riboside
Healthspan
Autophagy
Mitochondria

ABSTRACT

Replication stress, caused by *Rev1* deficiency, is associated with mitochondrial dysfunction, and metabolic stress. However, the overall metabolic alterations and possible interventions to rescue the deficits due to *Rev1* loss remain unclear. Here, we report that loss of *Rev1* leads to intense changes in metabolites and that this can be manipulated by NAD$^+$ supplementation. Autophagy decreases in *Rev1*$^{-/-}$ mouse embryonic fibroblasts (MEFs) and can be restored by supplementing the NAD$^+$ precursor nicotinamide riboside (NR). The abnormal mitochondrial morphology in *Rev1*$^{-/-}$ MEFs can be partially reversed by NR supplementation, which also protects the mitochondrial cristae from rotenone-induced degeneration. In nematodes *rev-1* deficiency causes sensitivity to oxidative stress but this cannot be rescued by NR supplementation. In conclusion, *Rev1* deficiency leads to metabolic dysregulation of especially lipid and nucleotide metabolism, impaired autophagy, and mitochondrial anomalies, and all of these phenotypes can be improved by NR replenishment in MEFs.

Research topic(s)

CP: Molecular biology.

1. Introduction

Maintaining genomic integrity is vital for the survival and health of organisms. The DNA repair machinery is tightly regulated and fixes endogenously and exogenously induced DNA damages. Less efficient or low-fidelity DNA repair is a major driving force for genomic instability, which further leads to aging and aging-related diseases [1]. Insufficient DNA repair such as gene mutations or loss of function also causes replication stress. In the context of UV-induced replication stress, regular replicative polymerases are exchanged

* Corresponding author.
E-mail address: lenera@sund.ku.dk (L.J. Rasmussen).
[1] These authors contributed equally to this work.

https://doi.org/10.1016/j.heliyon.2023.e17392
Received 12 January 2023; Received in revised form 13 June 2023; Accepted 15 June 2023
Available online 19 June 2023

for specialized translesion DNA synthesis (TLS) polymerases such as REV1, which is recruited to the replication arrest site, and directly interacts with monoubiquitinated PCNA [2]. Replication stress has crucial effects on cell survival, genome stability, mitochondrial maintenance, and human diseases [3,4]. Replication stress via loss of *Rev1* is associated with genome instability, mitochondrial alterations (bioenergetics, dynamics, and mitophagy), autophagy, and metabolic stress via alterations in nuclear-mitochondrial communication [5]. *Rev1*-deficient mice exhibit mild cytopenia and compromised proliferation and viability of hematopoietic stem cells (HSPC), which is associated with mitochondrial dysfunction [6]. Moreover, DNA replication stress increases the dNTP pool which leads to spontaneous mutations [7,8]. In turn, nucleotide imbalance leads to more replication stress [9], as well as mitochondrial dysfunction [10]. Interestingly, increased dNTP pools or treatment to induce the dNTP pool precursors in cancerous cells is associated with reduced autophagy [11]. Overall, there appear to be strictly regulated mechanisms that ensure communication between DNA metabolism in the nucleus and metabolic processes in the cytoplasm. Interestingly, *Rev1* knockout mice have lower lean mass accompanied by glucose intolerance. Furthermore, the mice were characterized by a mitochondrial energy deficit associated with increased anaerobic glycolysis and reduced locomotor activity. NAD^+ supplementation after the onset of metabolic dysfunction did not rescue this phenotype [12].

NAD^+ plays a critical role in the TCA cycle, oxidative phosphorylation (OXPHOS), and acts as a co-factor for cellular homeostasis [13–15]. The decline in NAD^+ leads to altered metabolism in aging and age-related diseases [16–20]. DNA damage repair is an energy-consuming process and the proteins involved in this process are dysregulated in some diseases, such as cancer, neurodegenerative diseases, and diabetes, involving alterations in post-translational modifications including PARylation, acetylation, and deacetylation [21]. One of the NAD^+ consumers, Poly [ADP-ribose] polymerase 1 (PARP1), is recruited to DNA damage sites during single and double-strand break repair [22]. Activation of PARP1 confers PARylation of itself and other proteins, affecting the nuclear deacetylase protein, SIRT1, which competes for NAD^+ with PARP1 [23]. Hyperactivation of PARP1 increases the catalysis of NAD^+ to NAM and ADP ribose. NAM inhibits the expression of the NAD^+-dependent deacetylase, SIRT1 [24]. Persistent PARP1 activation along with NAD^+ depletion increases PARylation in Xeroderma pigmentosum Group A (XPA) [25], Cockayne syndrome (CS) [26], and Alzheimer's disease (AD) models [27]; and replenishment of NAD^+ by NAD precursors, such as nicotinamide riboside (NR) and nicotinamide mononucleotide (NMN), can reverse these alterations [25,28]. Besides, PARP1 activation also leads to mitochondrial dysfunction [25,29,30].

Our previous study shows that *Rev1*$^{-/-}$ MEFs display hyperactivation of PARP1, NAD^+ depletion, decreased AMPK, SIRT1 expression, and mitochondrial dysfunction [5] Here, we demonstrate that *Rev1* deficiency causes a metabolic shift including decreased NAD^+ metabolism as well as increased nucleotide, phospholipids, sphingolipids, and ceramides synthesis. These changes likely influence the dysregulation of mitochondrial homeostasis in *Rev1*-deficient MEFs since they can be rescued by the replenishment of NR in MEFs. This study provides new insights into the intersection between DNA damage repair, autophagy, and metabolism.

2. Results

2.1. *Metabolism is altered in Rev1*$^{-/-}$ *MEFs*

Rev1 deficiency induces replication stress to cause metabolic dysfunction in mice [6,12] suggesting an interaction between genomic instability and cellular metabolism. Therefore, we asked whether *Rev1* deficiency would cause dysregulation or changes in specific metabolic pathways. We examined the metabolome of wildtype and *Rev1*$^{-/-}$ MEFs with and without NR supplementation (Fig. 1).

Multivariate analysis using Partial Least Square Discriminate Analysis (PLS-DA) resulted in the visual separation of the metabolomes in multidimensional space, which clearly showed that the metabolite profiles were different in *Rev1*$^{-/-}$ compared to wildtype

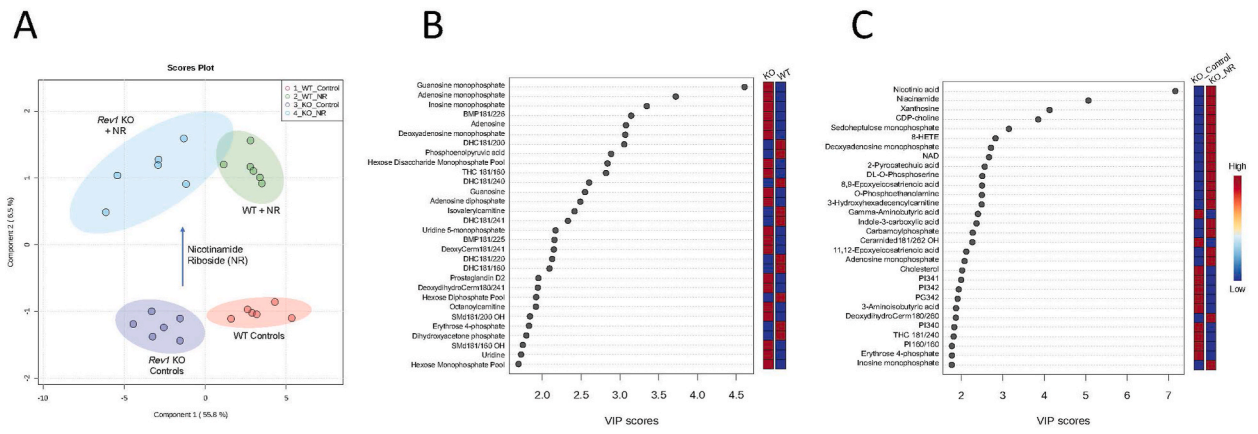

Fig. 1. Metabolome analysis of wildtype and *Rev1*$^{-/-}$ MEFs treated with or without nicotinamide riboside (NR).
(A) The four different clusters were plotted. **(B)** Significantly altered metabolites between wildtype and *Rev1* deficient cells were ranked. **(C)** Ranked metabolites between *Rev1*$^{-/-}$ MEFs treated with or without NR. Metabolites with importance in the projection (VIP) scores>1.2 were considered as significant contributors.

Table 1
Metabolic pathways in mouse embryo fibroblasts changed by Rev1 knockout compared to wild-type controls.

No.	Pathway Name	Measured Metabolites in the Pathway (N)	Expected Pathway Proportion (P] N/474)	Expected Hits in Sample of 80 (P * 80)	Observed Hits in the Top 80 Metabolites	Fold Enrichment (Obs/Exp)	Hypergeometric p Value	Impact (Sum VIP)	Fraction of Impact (VIP) Explained (% of 143.39)	Increased	Decreased
1	Purine Metabolism	30	0.06	5.1	10	2.0	0.02	27.3	19%	10	0
2	Phospholipid Metabolism	75	0.16	12.7	13	1.0	0.51	20.3	14%	12	1
3	Sphingomyelin Metabolism[a]	38	0.08	6.4	13	2.0	0.01	19.0	13%	13	0
4	Glycosphingolipid Metabolism[a]	18	0.04	3.0	6	2.0	0.07	15.0	11%	1	5
5	Glycolysis and Gluconeogenesis Metabolism	13	0.03	2.2	5	2.3	0.05	9.5	7%	2	3
6	Deoxysphingolipids[a]	9	0.02	1.5	6	4.0	0.001	9.4	7%	6	0
7	Pyrimidine Metabolism	25	0.05	4.2	5	1.2	0.42	8.2	6%	4	1
8	Amino-Sugar, Galactose, & Non-Glucose	7	0.02	1.2	3	2.5	0.10	5.9	4%	3	0
9	Fatty Acid Oxidation and Synthesis	32	0.07	5.4	3	0.6	0.93	4.6	3%	3	0
10	Ceramide Metabolism[a]	28	0.06	4.7	3	0.6	0.88	3.9	3%	3	0
11	Bioamines and Neurotransmitter Metabolism	9	0.02	1.5	2	1.3	0.47	2.9	2%	2	0
12	Ubiquinone and Dolichol Metabolism	4	0.01	0.7	2	3.0	0.13	2.8	2%	2	0
13	Branch Chain Amino Acid Metabolism	11	0.02	1.9	1	0.5	0.87	2.4	2%	0	1
14	Eicosanoid and Resolvin Metabolism	14	0.03	2.4	1	0.4	0.93	2.0	1%	1	0
15	Pentose Phosphate, Gluconate Metabolism	5	0.01	0.8	1	1.2	0.61	1.8	1%	0	1
16	Vitamin D (Calciferol) Metabolism	2	0.004	0.3	1	3.0	0.31	1.7	1%	1	0
17	Vitamin B3 (Niacin, NAD+) Metabolism	6	0.01	1.0	1	1.0	0.67	1.6	1%	0	1
18	Gamma-Glutamyl and other Dipeptides	4	0.01	0.7	1	1.5	0.52	1.3	1%	0	1
19	Cardiolipin Metabolism	3	0.01	0.5	1	2.0	0.43	1.3	1%	1	0
20	Lysine Metabolism	3	0.01	0.5	1	2.0	0.43	1.3	1%	1	0
21	Cholesterol, Cortisol, Non-Gonadal Steroid	8	0.02	1.4	1	0.7	0.78	1.2	1%	1	0

[a] Sphingolipids.

Table 2
Metabolic pathways in Rev1 knockout mouse embryo fibroblasts changed by nicotinamide riboside treatment.

No.	Pathway Name	Measured Metabolites in the Pathway (N)	Expected Pathway Proportion (P] N/474)	Expected Hits in Sample of 70 (P * 70)	Observed Hits in the Top 70 Metabolites	Fold Enrichment (Obs/Exp)	Hypergeometric p Value	Impact (Sum VIP)	Fraction of Impact (VIP) Explained (% of 134.86)	Increased	Decreased
1	Phospholipid Metabolism	75	0.16	11.1	17	1.5	0.0	30.3	23%	4	13
2	Vitamin B3 (Niacin, NAD+) Metabolism	6	0.01	0.9	4	4.5	0.0	16.1	12%	3	1
3	Purine Metabolism	30	0.06	4.4	7	1.6	0.1	14.7	11%	6	1
4	Eicosanoid and Resolvin Metabolism	14	0.03	2.1	6	2.9	0.0	12.1	9%	6	0
5	Pyrimidine Metabolism	25	0.05	3.7	5	1.4	0.3	7.9	6%	1	4
6	Benzoate and Indole Metabolism	22	0.05	3.2	4	1.2	0.4	7.6	6%	4	0
7	Glycosphingolipid Metabolism	18	0.04	2.7	4	1.5	0.3	6.2	5%	0	4
8	Fatty Acid Oxidation and Synthesis	32	0.07	4.7	3	0.6	0.9	5.6	4%	3	0
9	Pentose Phosphate, Gluconate Metabolism	5	0.01	0.7	2	2.7	0.2	4.9	4%	1	1
10	Glycolysis and Gluconeogenesis Metabolism	13	0.03	1.9	3	1.6	0.3	4.6	3%	1	2
11	Sphingomyelin Metabolism	38	0.08	5.6	3	0.5	0.9	4.4	3%	1	2
12	Ceramide Metabolism	28	0.06	4.1	2	0.5	0.9	3.5	3%	0	2
13	Cholesterol, Cortisol, Non-Gonadal Steroid Metabolism	8	0.02	1.2	2	1.7	0.3	3.5	3%	1	1
14	Deoxysphingolipids	9	0.02	1.3	2	1.5	0.4	3.3	2%	2	0
15	Bioamines and Neurotransmitter Metabolism	9	0.02	1.3	2	1.5	0.4	2.8	2%	0	2
16	1-Carbon, Folate Metabolism	9	0.02	1.3	1	0.8	0.8	2.5	2%	1	0
17	GABA, Glutamate, Arginine, Ornithine, Proline	7	0.02	1.0	1	1.0	0.7	2.4	2%	0	1
18	Nitric Oxide, Superoxide, Peroxide Metabolism	4	0.01	0.6	1	1.7	0.5	1.3	1%	1	0
19	Endocannabinoid Metabolism	3	0.01	0.4	1	2.3	0.4	1.2	1%	1	0

cells (Fig. 1A). NR treatment had a significant effect on the metabolite profiles in both the *Rev1*$^{-/-}$ and wildtype cells (Fig. 1A).

We found that *Rev1*$^{-/-}$ cells show significantly altered metabolites mainly in purine, pyrimidine, phospholipid, sphingolipid, glucose, and vitamin metabolic pathways, as compared to wildtype cells (Table 1). Twenty-one metabolic pathways were significantly altered in *Rev1*$^{-/-}$ cells. Purine metabolism was the most changed. About 19% of the total metabolic impact was contributed by changes in purines. All 10 of 10 purines that were changed were increased. These included increased guanosine monophosphate, adenosine monophosphate, inosine monophosphate, adenosine, guanosine, adenosine diphosphate, and guanosine diphosphate (Fig. 1B, Table 1). Several of these metabolites have been linked to protection of glial cells during glucose deprivation and mitochondrial respiratory chain inhibition [31]. *Rev1* KO MEF cells showed increased deoxynucleotide metabolites such as dAMP and dGMP, which may be cytotoxic [32] The pyrimidine metabolites, uridine monophosphate, uridine diphosphate, uridine, and thiamine were all increased, while deoxyuridine was decreased (Fig. 1B, Supplementary Tables S1 and S2).

Four classes of sphingolipids contributed over 34% of the metabolic impact in *Rev1*$^{-/-}$ cells. These included changes in sphingomyelins (13%), glycosphingolipids (11%), deoxysphingolipids (7%), and ceramides (3%) (Table 1). All 13 of 13 sphingomyelins that were changed were increased. These included SMd18:1/20:0 OH, SMd18:1/16:1 OH, SMd18:1/22:0, and SMd18:1/16:0 OH. We also found increases in deoxysphingolipids like deoxyceramide 18:1/24:1, and ceramides like ceramide d18:1/24:1. Increased deoxydihydroceramide is associated with diabetic neuropathy in type 2 diabetes and obesity [33]. Furthermore, increased plasma levels of select deoxy-ceramide and ceramide species are associated with diabetic neuropathy in type 1 diabetes [34]. Interestingly, *Rev1*-deficient mice revealed increased body weight, reduction of lean mass, and increased glucose intolerance [12]. Of the 4 classes of sphingolipids changed by *Rev1* knockout, only the glycosphingolipids were decreased, including the dihexosylceramides DHC18:1/20:0, and DHC18:1/24:0 (Fig. 1B, Supplementary Table S2). Dihexosylceramides, including lactosylceramide are enriched

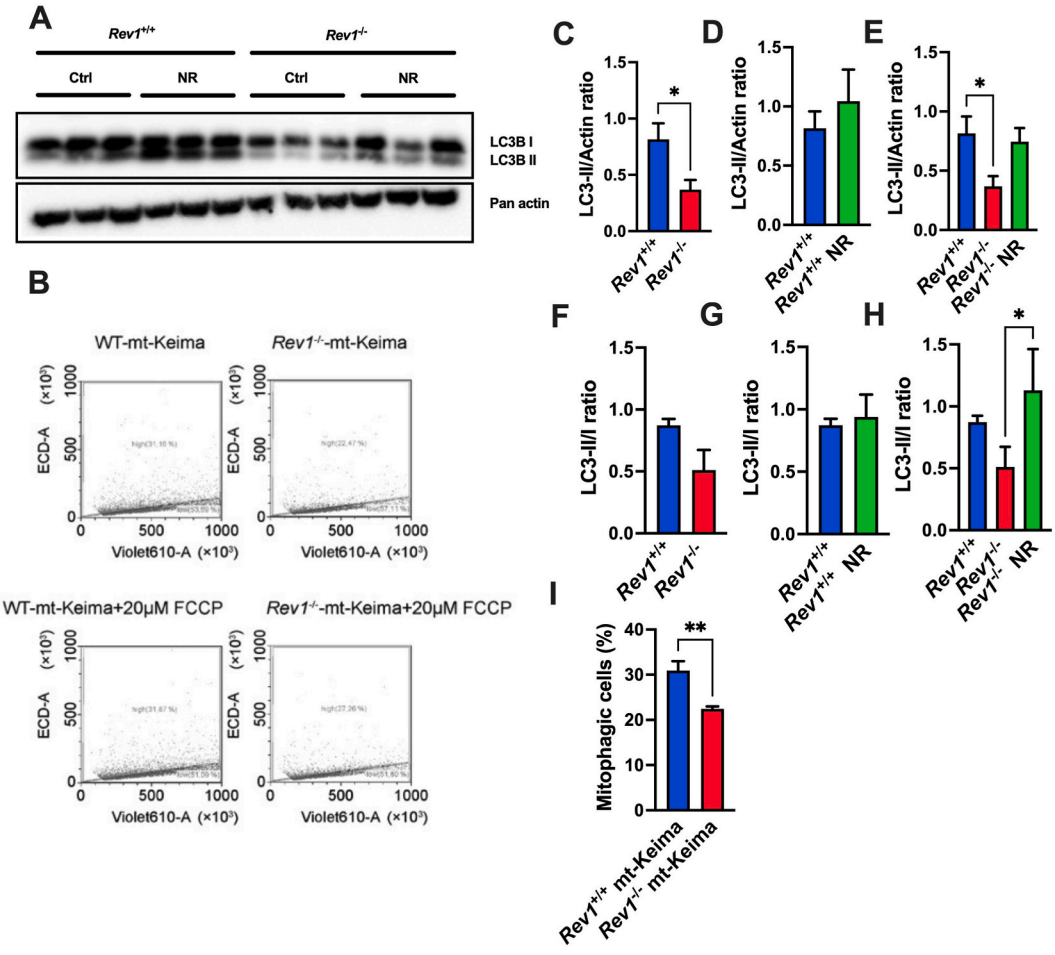

Fig. 2. Autophagy and mitophagy defects in *Rev1*$^{-/-}$ MEFs.
(A) Wildtype and *Rev1*$^{-/-}$ MEFs were treated with or without NR. LC3 was used as a marker for autophagy. N = 3. The full, non-adjusted image is shown in Supplementary Fig. 2A. (B) To measure mitophagy we used a pH-dependent fluorescence assay based on the coral-derived protein Keima, Wildtype and *Rev1*$^{-/-}$ MEFs integrated with mt-mKeima were treated with 20 μM FCCP to induce mitophagy. Cells were analyzed by flow cytometry. (C) Quantification of LC3-II/ACTIN in panel A. (D,E) Quantification of LC3-II/Actin ratios in panel A. (F–H) Quantification of LC3-II/I ratios in panel A. (I) Quantification of mitophagic cells in panel B. N = 3. Data is presented as mean ± SEM. *$p < 0.05$; **$p < 0.01$.

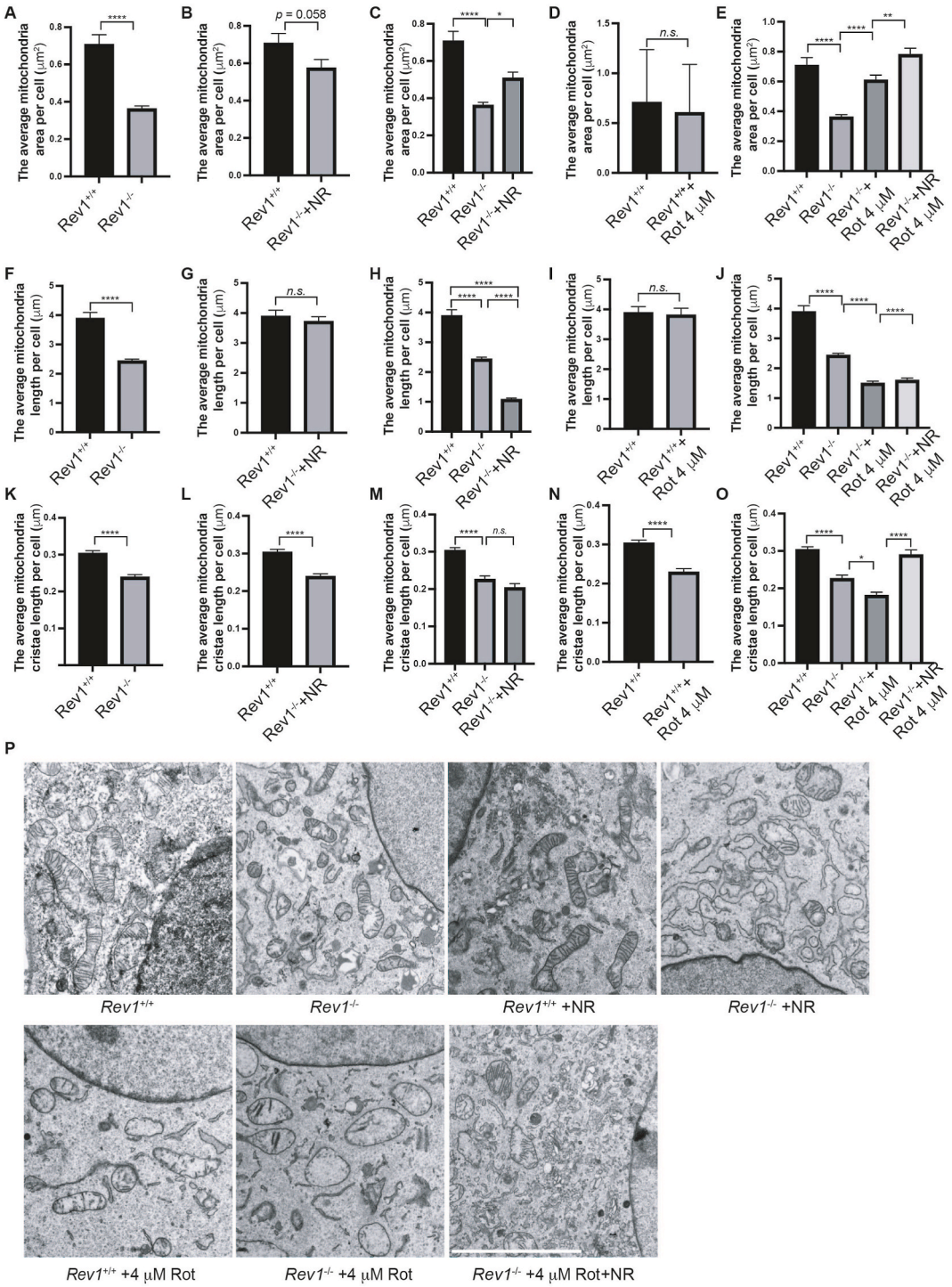

Fig. 3. Electron microscope analysis of MEFs treated with rotenone and/or NR.
Wildtype and *Rev1*$^{-/-}$ MEFs were treated with NR or rotenone or the combination of NR or rotenone. NR (3 mM, 18 h), rotenone (Rot, 4 μM, 12 h), and quantification of mitochondrial area, length and cristae length was done using Image J. The average mitochondria area, the average mitochondria length and the average of mitochondria cristae length per cell was obtained by counting three cells under different conditions individually. Randomly ten images were used for mitochondrial area and length quantification, and twenty images were used for the quantification of cristae length. (**A**), (**B**), (**C**), (**D**), (**E**): The average mitochondria area was quantified under different conditions. (**F**), (**G**), (**H**), (**I**), (**J**): The average mitochondria length was quantified under different conditions. (**K**), (**L**), (**M**), (**N**), (**O**): The average mitochondria cristae length was quantified under different conditions. (**P**) The representative electron microscopy images were shown under different conditions. Scale bar, 2 μm. Data are presented as mean ± SEM. *$p < 0.05$; **$p < 0.01$; ****$p < 0.0001$.

in membrane lipid rafts and play essential roles in innate immunity through neutrophil function, and adaptive immunity through T cell selection [35].

Changes in phospholipid metabolism contributed 14% of the metabolic impact (Table 1, Supplementary Table S2). Twelve of the 13 (92%) phospholipids that were changed in *Rev1*$^{-/-}$ cells were increased. These included several phosphoinositol lipids involved in calcium signaling like PI36:2, PI36:4, PI38:4, and PI36:1, and bis(monoacylglycero) phosphates like BMP18:1/22:6, and BMP18:1/22:5. BMP lipids are involved in lysosomal trafficking and are upregulated in secreted exosomes in response to defects in autophagy [36].

Our results show that specific glucose, vitamins, and amino acid metabolites increase in *Rev1*$^{-/-}$ compared to wildtype MEFs. These include hexose monophosphates and disaccharides, prostaglandin, octanoylcarnitine, vitamin D3, N-acetyl-glucosamine-1-phosphate, and L-aspartic acid. However, other metabolites associated with glucose, NAD$^+$, and vitamin metabolism were decreased in *Rev1*$^{-/-}$ MEFs, including phosphoenolpyruvate, isovalerylcarnitine, hexose diphosphate, erythrose 4-phosphate, dihydroxyacetone, and 1-methyl nicotinamide (Fig. 1B, Supplementary Table S2).

Phospholipid metabolism was the top pathway that was most changed by NR treatment, contributing over 22% of the metabolic impact (Table 2, Supplementary Table S3). Treating *Rev1*$^{-/-}$ cells with NR decreased several phosphoinositol (PI) phospholipids that were previously elevated such as PI34:1, PI36:1, and PI36:2. NR treatment also increased CDP-choline levels that were previously decreased. In *Rev1*$^{-/-}$ MEFs, 1-methylnicotinamide as a marker of vitamin B3 (Niacin, NAD$^+$) metabolism, was significantly decreased (Table 1, Fig. 1B, Supplementary Table S2). Interestingly, the premature aging syndrome Werner knockout cells also show decreased 1-methylnicotinamide metabolite compared to wildtype [19]. Furthermore, *Rev1* KO mice show signs of premature aging and shorter lifespan than their wildtype littermates [6]. Supplementation with NR increased three of six measured metabolites in vitamin B3 metabolism. Increased NR metabolites were nicotinic acid, niacinamide, and NAD$^+$ (Table 2). NADH in comparison, was decreased after NR supplementation. Pentose phosphate and gluconate metabolism were decreased and fatty acid oxidation and synthesis were increased (Table 1). The pentose phosphate pathway is a pathway used for NADPH production and biosynthesis of fatty acids and the nucleotide precursor ribose [37]. The five most significantly altered metabolites between *Rev1*$^{-/-}$ cells treated with and without NR supplementation were nicotinic acid, niacinamide, xanthosine, CDP-choline, and sedoheptulose (Fig. 1C). Pyrimidine metabolites were decreased and eicosanoid and resolvin metabolites were increased (Table 2) in *Rev*$^{-/-}$ MEF cells treated with NR compared to the untreated controls.

In conclusion, we found that *Rev1* deficiency causes comprehensive alterations in cellular metabolites, particularly in nucleotide (purines and pyrimidines), lipid metabolites, and NAD$^+$ metabolism. The *Rev1*$^{-/-}$ cells compared to wildtype have several features of metabolic syndrome. This includes elevations in purines, phospholipids, sphingolipids, and cholesterol. Interestingly, NR supplementation could restore many of the metabolite changes observed in *Rev1*$^{-/-}$ cells but not all.

2.2. Compromised autophagy is rescued by NR supplementation in MEFs

Our metabolomics analysis indicates that *Rev1*$^{-/-}$ MEFs show metabolic alterations in nucleotide and lipid biosynthesis, and these alterations might affect mitochondrial functions. The depletion of NAD$^+$ metabolites decreases autophagy and mitophagy, which has been implicated in aging and aging-related diseases [38] and is also observed in *Rev1*$^{-/-}$ MEFs [5]; (Fig. 1). Given that the NAD$^+$ metabolism is augmented in *Rev1*$^{-/-}$ cells after NR supplementation, we asked whether the increase of NAD$^+$ metabolites would rescue the decreased autophagy/mitophagy (Fig. 2). We examined autophagy by detecting the protein expression of the autophagy marker LC3, and quantifying the ratio of LC3-II to LC3-I in wildtype and *Rev1*$^{-/-}$ MEF cells. *Rev1*$^{-/-}$ cells showed a decrease in LC3-II expression and LC3-II/LC3-I ratio compared to wildtype cells, indicating compromised autophagy (Fig. 2A,C,F). The autophagy defects were reversed by supplementing with 3 mM of NR for 30 h (Fig. 2D,E,G,H). There is no significant difference of NR supplementation on autophagy in wildtype MEFs under the experimental conditions used in this study (Fig. 2D,G). Next, we evaluated mitophagy using the mt-mKeima [39]. *Rev1*$^{-/-}$ cells show a decreased proportion of mitophagic cells compared to wild-type cells (Fig. 2B,I).

Taken together, we show that replication stress-mediated dysregulation of NAD$^+$ metabolism impairs autophagy and mitophagy in *Rev1*$^{-/-}$ MEFs. This can be reversed by supplementation of NR via remodeling NAD$^+$ metabolism.

2.3. Impaired mitochondrial dynamics is reversed by NR supplementation in MEFs

Defective autophagy and mitophagy can cause the accumulation of dysfunctional mitochondria, which can influence the pathogenesis of many age-related diseases. This will worsen if there is an increase in dysfunctional mitochondria. Mitochondrial dynamics comprises mitochondrial morphology such as number, size, and cristae [40]. Our previous work showed that mitochondrial function was impaired and mitochondria were more fragmented or elongated in *Rev1*$^{-/-}$ MEFs and murine hepatocytes [5]. To further investigate the mechanisms underlying dysfunctional mitochondria, we examined mitochondrial morphological parameters changes using transmission electron microscopy (TEM). Mitochondrial parameters in *Rev1*$^{-/-}$ cells compared to wildtype cells show that mitochondrial area, length, and length of cristae decreased significantly (Fig. 3A,F,K). These results suggest that *Rev1*-deficient cells have smaller mitochondria with fewer cristae compared to wildtype MEFs. The smaller and fragmented mitochondria are in concert with the increased DRP1 phosphorylation and activation in *Rev1*$^{-/-}$ MEFs [5], which contributes to the enhancement of fission in these cells. In wildtype MEFs supplementation with 3 mM NR for 30 h showed a significant decrease in cristae length (Fig. 3B,G,L). In *Rev1*$^{-/-}$ MEFs, there was a decrease in mitochondrial number (data not shown), length and area of mitochondria as well as the length of cristae (Fig. 3C,H,M). In *Rev1*$^{-/-}$ MEFs, mitochondrial length decreased after NR treatment (Fig. 3H) whereas as mitochondrial area significantly increased after NR treatment (Fig. 3C). To investigate the benefits of NR supplementation for mitochondrial protection,

the Complex I inhibitor rotenone was used to stress the cells. After treatment with 4 μM rotenone for 12 h, we did not detect any significant effects on wildtype cells except for the decreased cristae length compared to the untreated control (Fig. 3D,I,N). On the other hand, the *Rev1*$^{-/-}$ cells show increased mitochondrial area (Fig. 3E) and a significant decrease in mitochondrial length and cristae length after rotenone treatment (Fig. 3J,O). *Rev1*$^{-/-}$ cells pretreated with 3 mM NR for 18 h and then treated with 4 μM rotenone show a significant recovery of mitochondrial area and cristae length compared to rotenone treatment in *Rev1*$^{-/-}$ cells (Fig. 3E,O). Our results show that mitochondrial morphology is altered in *Rev1*-deficient MEFs and mitochondrial morphology changes in *Rev1*-deficient cells is more sensitive to rotenone treatment. Interestingly, rotenone-induced mitochondria morphology changes such as mitochondria area and length of cristae can be reversed by NR supplementation in *Rev1*$^{-/-}$ MEFs.

2.4. *Rev1 deficiency does not affect lifespan and healthspan in C. elegans*

C. elegans has been used as a model system for studies on aging, age-related diseases, and mechanisms of longevity in recent decades. This is based on its physiological aging characteristics. Therefore, we used this model to investigate role of Rev1 deficiency in vivo. In *C. elegans* models, NAD^+ depletion, mitochondrial dysfunctions, and alteration of mitochondrial dynamics affect lifespan and healthspan [29]. Our previous work also shows a shortened lifespan in *Rev1*$^{-/-}$ mice compared to their wildtype siblings [6]. Our metabolomics results show decreased NAD^+ metabolites in *Rev1*$^{-/-}$ MEFs and that supplementation of NAD^+ precursor restores NAD^+ metabolites (Fig. 1A, C). Based on these results and the observation that NR supplementation partly suppresses changes in mitochondrial morphology in *Rev1*$^{-/-}$ MEF cells (Fig. 3E,O), we further asked whether *Rev1* deficiency would affect life- and healthspan in a nematode model. The *rev-1* gene in *C. elegans* is a homolog of mouse *Rev1*, which is involved in TLS upon UV damage [41,42]. We used a *rev-1 C. elegans* mutant carrying a deletion of *rev-1* (exon 2). This strain is sensitive to UV irradiation [42] (Fig. 4A and B) and undergoes replication stress upon UV damage. Since unrepaired DNA damage induces PARP1 and depletes NAD^+ pools, we treated

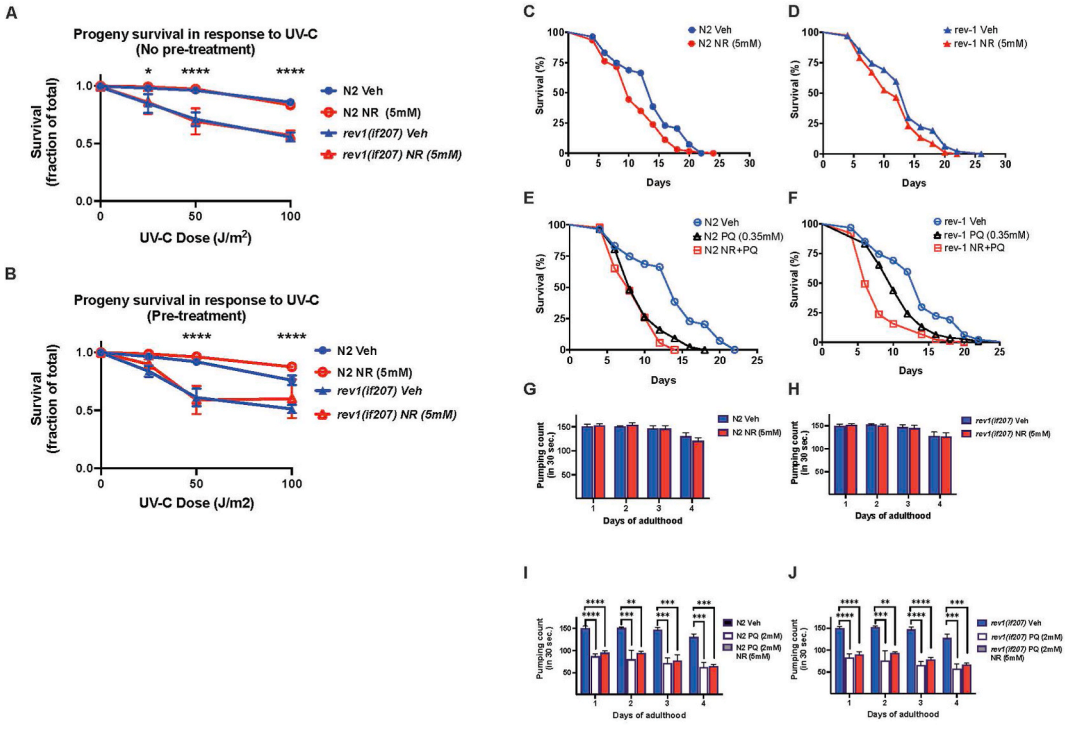

Fig. 4. Lifespan and healthspan of wildtype N2 and *rev-1*-deficient *C. elegans*.
Progeny survival in response to UV-C exposure of adult hermaphrodites. NR was supplemented from the day 1 adult stage **(A)** or the L4 stage **(B)** and throughout the 24 h of egg laying and subsequent hatching of eggs (statistical difference is noted for differences between N2 and *rev-1(If207)* animals). Lifespan was measured for N2 **(C)** and *rev-1(If207)* **(D)** with and without NR supplementation (5 mM). Lifespan was measured for N2 **(E)** and *rev-1(If207)* **(F)** with and without paraquat aa well as with paraquat + NR. The worms were treated in the L4 larval stage either as vehicle, 5 mM NR, 0.35 mM Paraquat or Paraquat + NR for each genotype, N2 and *rev-1*(*If207*). The counting was done from day 1 adult and continued every second day until end of lifespan. On 2ndday the worms were transferred to new plates prepared with the corresponding treatments. Healthspan was measured as the pharynx pumping counts for 30 s every day over 4 days. Both N2 **(G)** and *rev-1*(If207) **(H)** were supplemented with NR. NR N2 **(I)** and *rev-1*(If207) **(J)** were also treated with paraquat and paraquat + NR. The worms were treated in the L4 larval stage either as vehicle, 5 mM NR, 2 mM Paraquat or Paraquat + NR for each genotype, N2 and *rev-1*(If207). The counting was done from day 1 adult to day 4 adult. On day 2 the worms were transferred to new plates prepared with the corresponding treatments. Data is presented as mean ± SD. N = 3, ****p < 0.0001 ***p < 0.001 **p < 0.01.

nematodes with NR to investigate if the UV sensitivity of *rev-1* nematodes could be suppressed by increasing NAD $^+$ levels. We used two different protocols, without NR pretreatment (Fig. 4A) and with NR pretreatment (Fig. 4B). Our results show that *rev-1* deficiency sensitizes nematodes to UV damage and that NR supplementation does not suppress this phenotype (Fig. 4A and B). This result suggests that unrepaired UV damage does not deplete NAD^+ levels, at least not enough, to cause a shorter lifespan induced by NAD $^+$ supplementation in the *rev-1* nematode model.

To investigate if Rev1 and NAD $^+$ levels regulate lifespan we followed the lifespan of N2 and *rev-1* nematodes from the L4 stage untreated or treated with 5 mM of NR (Fig. 4C and D). There was no significant difference in the lifespan of N2 nematodes treated with NR, compared to untreated controls (Fig. 4C and D). Paraquat is known to induce oxidative stress and induce replication stress. Accordingly, treatment with paraquat shortened the lifespan of both N2 and *rev-1*-deficient nematodes and this could not be suppressed by NR supplementation (Fig. 4E and F). Along these lines, we did not detect any differences in healthspan of N2 and *rev-1*-deficient nematodes treated with paraquat and NR (Fig. 4G–J). Overall, our results show that *Rev1* deficiency does not shorten the lifespan in nematodes as it does in mice.

3. Discussion

Here we report that loss of *Rev1* causes significant changes in the metabolome. These alterations include changes in nucleotide/lipid metabolism, and decreased NAD $^+$ metabolism. The increased nucleotide biosynthesis is in line with the increased replication stress in *Rev1*$^{-/-}$ cells. Besides, this is also an explanation of why autophagy is compromised in *Rev1* knockout cells as dNTP supplementation decreases autophagy induction in cancer cells [11]. Decreased NAD^+ metabolites are involved in aging and aging-related diseases, such as Alzheimer's disease, cancer, diabetes, ataxia-telangiectasia, and WRN syndrome [17,43]. Here, we reveal that NAD^+ augmentation by supplementation of NR results in enhanced NAD^+ metabolism including a decrease in pyrimidine, phospholipids, sphingolipids, and ceramides metabolism. Sphingolipids are not only involved in cell membrane structure formation, but also play crucial roles in cell signaling, mitochondrial dynamics, and mitophagy process [44]. Besides, many sphingolipid metabolic pathway enzymes are translocated to mitochondria [44]. The increased phospholipids, sphingomyelin, and ceramides in *Rev1*$^{-/-}$ cells were widely observed in numerous metabolic and inflammatory disorders [45,46]. SM(d18:1/16:0) (a specific sphingomyelin species) is accumulated in diabetic kidney accompanied by decreased AMPK activity and PGC-1α protein expression [47]. While suppression of sphingomyelin synthases relieves the inhibition of AMPK and PGC-1α and the exogenous addition of SM(d18:1/16:0) metabolite *in vitro* increases glucose consumption and lactate production [47]. This links increased sphingomyelin to decreased AMPK phosphorylation [5].

Increased genomic stress due to loss of Rev1, exacerbates the utilization of energy metabolites, such as NAD^+ and ATP, which is likely the reason why *Rev1*$^{-/-}$ MEFs show a decrease in NAD^+ metabolites compared to wildtype cells (Fig. 1, [5]). Depletion of Rev1 has been shown to alter NAD^+ levels, which can affect mitochondrial function, and autophagy/mitophagy; while NAD^+ supplementation can reverse the mitochondrial respiratory and autophagy defects (Fig. 2, [5]). Increasing NAD^+ levels in WRN also show improved mitophagy [38]. NAD^+ is an essential cofactor in many processes, and imbalances in the NAD^+ level decrease SIRT1 level and AMPK activity through hyperactivation of PARP1 and impairment of mitochondrial dynamics [5]. AMPK controls energy expenditure by increasing cellular NAD^+ levels to augment SIRT1 activity [48]. *Rev1*$^{-/-}$ MEFs show several changes in mitochondrial morphology and NR supplementation suppresses some of these phenotypes (Fig. 3P). Unlike mice, in *C. elegans* life and healthspan were not affected by *Rev1* deficiency. DNA damage decreased life- and healthspan of *Rev1*-deficient nematodes but NR supplementation did not suppress these phenotypes (Fig. 4). Also, NR supplementation does not rescue the metabolic phenotype of female Rev1 KO mice measured as improvement of adiposity or glucose tolerance. These results suggest that Rev1-mediated NAD^+ depletion is tissue and/or cell type specific [12]. These results reveal an interesting and complex interaction between nuclear and mitochondrial phenomena that involves the controlled action of cellular metabolites.

In conclusion, we show that in MEFs, *Rev1* deficiency causes metabolic changes including mitochondrial dysfunction, which can be manipulated by increasing NAD^+ levels. In nematodes, *rev-1* deficiency and NR supplementation do not affect life- and healthspan as shown in mice [6]. This suggests significantly different mechanisms underlying the role of Rev1 in longevity in mice and nematodes. This study provides new insights into the intersection between DNA damage repair, autophagy, and metabolism. However, the underlying mechanisms remain unclear. In MEFs we have shown that replication stress via Rev1-deficiency contributes to metabolic stress caused by compromized mitochondrial function via this PARP-NAD + -SIRT1-PGC1α axis [5].

4. STAR★Methods

4.1. Experimental model and subject details

4.1.1. Cell culture

Wildtype and *Rev1*$^{-/-}$ MEFs have been described previously [6,49]. Cells were cultured in Dulbecco's Modified Eagle Medium (DMEM) plus 10% (v/v) fetal bovine serum (Invitrogen) and 100 U/mL penicillin/streptomycin (Thermo Fisher Scientific, #15140122), in an incubator with 5% CO_2 at 37 °C.

4.1.2. Antibodies

LC3B/MAP1LC3B (Novus Biologicals, #NB100-2220) (1:1000); pan-Actin (Thermo Fisher Scientific, #MA5-11869) (1:10,000); AMPKα (Cell signaling, #2532) (1:1000); Phospho-AMPKα (Thr172) (Cell signaling, #2531) (1:1000); DRP1 (Cell signaling, #8570)

(1:1000); Phospho-DRP1 (Ser616) (Cell signaling, #3455) (1:1000).

4.1.3. Western blot

MEFs were lysed and resuspended in RIPA buffer (Sigma) supplemented with cOmplete™, EDTA-free Protease Inhibitor Cocktail (Sigma), and PhosSTOP phosphatase inhibitor Cocktail (Sigma). The cell suspension was incubated on ice by shaking on a shaker for 30 min. Subsequently, the cell suspension was centrifuged at 15,000 G-force for 15 min, and the supernatant was mixed with NuPAGE® LDS Sample Buffer (4 ×) (Thermo Fisher Scientific). Samples for gel electrophoresis were denatured at 95 °C for 5 min and 20–30 μg protein was resolved by NuPAGE™ Novex™ 4–12% Bis-Tris Protein Gels, 1.0 mm (Thermo Fisher Scientific) according to the manufacturer's instructions.

4.1.4. Metabolome sample preparation and analysis

For the metabolomics study 300,000 cells/15 cm dishes were plated on Day 0 (Non-critical cells) labeled as "Wildtype C57BL/6 ('B6') MEFs without NR", "Wildtype B6 with NR", "*Rev1*$^{-/-}$ MEFs without NR" and "*Rev1*$^{-/-}$ MEFs with NR"; 7 dishes for each experimental group were used as biological replicates. Cells were treated with 3 mM NR on day 1 and collected on day 4, from 6 biological replicates; a 7th replicate plate from each experimental group was processed for cell count using trypan blue viability after trypsinization. The rest of the 6 groups of cells were washed with 1 × PBS and the 1 × PBS was aspirated completely. Subsequently, dishes with cells were frozen and stored at −80 °C, tightly wrapped in aluminum foil. The following day, 100 mL of an 80:20 Methanol: Water solution was prepared (80% methanol:20% water) freshly and stored at −20 °C; 2 mL of this solution was added to the dishes previously stored at −80 °C, which were kept on ice. Next, cells were harvested by scraping and transferred into pre-labeled 2 mL Eppendorf tubes, vortexed and then snap-frozen in liquid nitrogen, thawed in cold water and vortexed again. This freeze-thaw cycle was repeated three times. 50 μL from each sample was collected and stored at −80 °C for Pico green assay. Remaining samples are centrifuged at 15,000 G for 10 min at 4 °C to precipitate proteins, DNA, RNA, and glycans. The supernatant extract from each plate was split into two (0.9 mL each) tubes and stored in labeled screw-cap cryotubes at −80 °C until they were processed at Naviaux Lab. Metabolomics was performed by high performance liquid chromatography tandem mass spectrometry (LC-MS/MS) as previously described [50]). Cell biomass was normalized by DNA content quantified by Pico green assay. Metabolite peak areas under the curve (AUCs) were log2 transformed for statistical analysis. Metabolites were scored according to their variable importance in the projection (VIP) scores using the PLS-DA model. Metabolites with VIP scores >1.2 were considered significant. Significant metabolites were aggregated into biochemical pathways and ranked by the sum of the VIP scores. Metabolomics data normalized for cell DNA content are reported in Supplementary Table S1.

4.1.5. Lentivirus packaging and infection

pHAGE-mt-mKeima was a gift from Richard Youle (Addgene plasmid, #131626 [39]). 293T cells are seeded in a 10 cm^2 dish. The next day, 293T cells reach 80% confluency which is suitable for transfection. For one 10 cm dish, mix 500 μL Opti-MEM™ Reduced Serum Medium (Thermo Fisher Scientific, #31985062) with plasmids (9 μg pCHAC-mt-mKeima, 4.5 μg pMDLg/pRRE, 4.5 μg pRSV-Rev, and 4.5 μg pMD2.G); mix 500 μL Opti-MEM with 67.5 μg PEI (polyethylenimine, transfection reagent, 1 μg/μL). Gently add the diluted PEI dropwise to the diluted DNA while gently swirling the tube with diluted DNA. Incubate the mixture for 15–20 min at room temperature. Then, the even transfection mixture is added dropwise to the 293T cell culture in a 10 cm^2 dish. The following morning, carefully replace the media with 10 mL of DMEM complete medium. Viral particles can be harvested at 48 h post-transfection. Collect and filter medium through a 0.45 μm sterile PES syringe filter. The viral supernatant can be stored at 4 °C for a short time, but it should be aliquoted and snap-frozen in liquid nitrogen and stored at −80 °C as soon as possible to avoid loss of titer for long-term storage. For lentivirus infection, wildtype and *Rev1*$^{-/-}$ cells are seeded one day before infection (Day −1). The next day (Day 0), mt-mKeima lentivirus is diluted with DMEM complete medium and added to cells. After 8 h, change medium with DMEM complete medium. Day 1, add 1.5 μg/mL puromycin to select the positive cells for 48 h. Finally, the stable mt-mKeima-integrated wildtype or *Rev1*$^{-/-}$ MEFs are generated.

4.1.6. Detection of mitophagy with FACS

To measure mitophagy we used a pH-dependent fluorescence assay based on the coral-derived protein Keima, which can be targeted to the mitochondrial matrix (mt-mKeima). The mt-mKeima probe enables differential imaging of mitochondria in the cytosol and mitochondria in autophagosomes/lysosomes, thus reflecting the underlying level of mitophagy. Mitophagy in *Rev1*$^{-/-}$ and wildtype MEF cells expressing mt-mKeima were evaluated by a FACS-based method. mt-mKeima-integrated wildtype or *Rev1*$^{-/-}$ MEFs were seeded in 12-well plates at a density of 5 × 10^4 cells/well and cultured for 24 h. Then, cells were treated with either 20 μM FCCP (Sigma-Aldrich, #C2920) or the same volume of DMSO for 3 h. Cells were trypsinized and mixed in 1 mL 1 × cold PBS to ensure singlets and put on ice. Wildtype or *Rev1*$^{-/-}$ MEFs without mt-mKeima integration were used as negative cells to set the gate for mt-mKeima positive cell detection by using the CytoFLEX S Flow Cytometer. The Violet610-A fluorescent channel is used to detect the green signals irradiated by 405 nm laser, while the ECD-A channel is used to detect the red signals irradiated by 561 nm laser. The mitophagy level is indicated by the ratio of ECD-A (561 nm)/Violet610-A (405 nm). The population with a higher ratio is designated as "high gate", while the population with a lower ratio as "low gate". A detailed protocol is available [51]. The ratio of Red to Green fluorescence intensity was used to denote mitophagy positive cells.

4.1.7. TEM samples preparation and analysis

Wildtype and *Rev1*$^{-/-}$ MEF cells were seeded on plastic coverslips in 24-well plate at a concentration of 2 × 10^3 cells per well and

cultured for 24 h at 37 °C in 5% CO2 incubator. Next day, wells were either supplemented with ("NR") or without ("Ctrl") 3 mM NR for 30 h; wells were treated with rotenone (either 2 μM or 4 μM) for 12 h ("Rot 2 μM" or "Rot 4 μM"); wells were supplemented with 3 mM NR for 18 h followed by rotenone treatment (either 2 μM or 4 μM) for the last 12 h of the total 30 h corresponding to approximate two cell divisions ("NR + Rot 2 μM" or "NR + Rot 4 μM"); wells were supplemented with 3 mM NR for 18 h followed by rotenone treatment (either 2 μM or 4 μM) combined with 3 mM NR for the last 12 h of 30 h ("NR + (NR + Rot 2 μM)" or "NR + (NR + Rot 4 μM)"). After 30 h, cells were washed twice with 1 × DPBS and fixed with 2% glutaraldehyde/0.1 M sodium cacodylate buffer (pH 7.4) at room temperature for 1 h. Thin sections were prepared by the Core Facility for Integrated Microscopy at the University of Copenhagen. All of the specimens are examined using a Transmission Electron Microscope Philips CM100, FEI. The effect of 3 mM and 5 mM NR treatment on mitochondrial function of MEFs has been described in Fakouri et al., [4]; data not shown.

4.1.8. Preparation of E. coli strain and plating on NGM plates for feeding C. elegans

The N2 Bristol strain was used as wildtype control. N2 (wildtype strain) and *rev-1(If207)*-deficient nematodes were obtained from Marcel Tijsterman (Leiden University, NL) [42].

Glycerol stock of OP50-1 *E. coli* strain (from CGC *C. elegans* library) resistant to streptomycin was streaked on an LB plate prepared with 50 μg/mL streptomycin (Sigma) and incubated overnight at 37 °C for single colony formation. The next day a single colony was picked and stirred in 100 mL of LB medium with 50 μg/mL of streptomycin and left at 37 °C for 12–14 h. 100 μL of the culture was added in the center of NGM 35 × 15 mm plates, or 200 μL in 60 mm NGM plates and plates were incubated for 2 days at room temperature to allow the bacterial lawn to grow.

4.1.9. Progeny survival in response to UV-C

A synchronous population of nematodes was made and about 30 L4 stage nematodes transferred to separate plates for each condition, which were treated with or without NR for a concentration of 5 mM NR. The following day in the young adult stage the plates were exposed to different doses of UV-C and 5 nematodes were picked randomly for each condition and put on separate plates which had been prepared either with or without NR according to the condition. After 24 h of laying eggs on the plates the adult nematodes were removed. After a further 24 h the amount of unhatched eggs and progeny was counted for each plate and the survival rate was calculated as $\frac{progeny}{progeny+eggs}$.

4.1.10. Synchronization of C. elegans

Wildtype and mutant nematodes were picked and transferred to five freshly seeded NGM plates (10 nematodes per plate) and incubated at 20 °C for 4–5 h to allow them to lay eggs. Next, adult nematodes were removed, and eggs were left on the continuation of the life cycle. In the next two days, they were incubated at 20 °C. From the synchronized nematodes, 12–15 L4 larval stage nematodes were picked per plate, and for each experimental group, three replicates were conducted.

4.1.11. Lifespan and healthspan assay

L4 larvae of N2 and *rev-1(If207)* mutant strains were transferred on to NGM plates with the OP50-1 bacterial strain at 20 °C. The plates were prepared either with FUDR (0.1 mg/mL) only or with FUDR (0.1 mg/mL) and 1 mM, 5 mM or 10 mM concentration of NR. Triplicates consisting of 12–15 L4 stage nematodes each were transferred to each experimental group, for both N2 and *rev-1*-deficient nematodes. The next day, nematodes were gently touched with a pick (made by using platinum wire), and the observation of whether they can move or not was used to score them as alive or dead. The scoring was done every alternative day until all experimental groups had no nematodes alive. Healthspan examination of *C. elegans* was performed described in Ref. [29] with nematodes on NGM with OP50-1 bacteria strain at 20 °C. Three NGM plates with 25 nematodes each were synchronized and left for three days to reach day 1 of adulthood. Examination of *C. elegans* healthspan was measured on synchronized nematodes by counting pharyngeal pumping for 20 s each time, five times per nematode, and five different nematodes every group. This was repeated until less than five nematodes were able to pump. We measured healthspan by counting pharyngeal pumping for 20 s, five times per nematode, in five different nematodes. NR supplementation was given on day 1, just before the measurement of pumping rates. We followed the healthspan of N2 and *rev-1*-deficient nematodes from day 1 of the adult stage in *C. elegans,* in the presence or absence of a 5 mM NR for 7 days (day 2-day 8) during which pumping can be easily recorded. The NAD + dependency and experimental conditions for NR treatment that improves the average lifespan and healthspan were determined on nematodes carrying mutated *dhs-3* gene.

4.2. Lifespan

A synchronous population of N2 and *rev-1(If207)* L4 nematodes was prepared. Plates were prepared with water, NR, paraquat and NR + paraquat at concentrations of 0.35 nM paraquat and 5 mM NR in the total volume of the growth medium in the plates. Around 30 L4 nematodes were placed on each plate, 3 plates per condition per genotype. Every second day the nematodes were moved to new plates which had been freshly prepared to the corresponding condition and simultaneously scored for whether they were alive.

4.3. Healthspan

4.3.1. 4 Days

NGM plates were treated with water, NR, paraquat or NR + paraquat respectively. Concentrations of NR and paraquat were 5 mM

and 2 mM in the total volume of the growth medium in the plate. Around 25–30 nematodes from a synchronous population of L4 nematodes were put on each plate, 3 plates per condition per genotype. The following day (day 1) adult 5 random nematodes on each plate were selected and the pumping of the pharynx was counted for 30 s and noted down. At day 2 adult the nematodes were transferred to freshly prepared plates with their corresponding conditions. Counting of the pumping was done every day from day 1 to day 4.

4.3.2. 10 Days

The 10 day healthspan was done simultaneously with the lifespan and was done the same way as for the 4 day healthspan besides the counting of additional days.

4.4. Statistical analysis

The difference between two groups was analyzed with unpaired Student's *t*-test. For the TEM images, data are shown as mean ± SEM. Group differences were analyzed with one-way or two-way analysis of variance (ANOVA) followed by Tukey's multiple comparisons test for multiple groups. All of the bar charts are prepared by using GraphPad Prism 8. $*p < 0.05$; $**p < 0.01$; $***p < 0.001$; $****p < 0.0001$. A multiple regression line analysis was performed for the healthspan of *C. elegans*.

Author contribution statement

Sharath Anugula, Zhiquan Li, Yuan Li, Alexander Hendriksen, Peter Bjarn Christensen, Lin Wang, Jonathan M. Monk, Robert K. Naviaux: Conceived and designed the experiments; Performed the experiments; Analyzed and interpreted the data; Wrote the paper.

Niels de Wind, Vilhelm A. Bohr, Claus Desler, Lene Juel Rasmussen: Conceived and designed the experiments; Analyzed and interpreted the data; Wrote the paper.

Funding statement

Dr Lene Juel Rasmussen was supported by Nordea-fonden, Olav Thon Stiftelsen, Novo Nordisk Fonden {NNF17OC0027812}.

Data availability statement

Data included in article/supp. material/referenced in article.

Declaration of competing interest

The authors have no Declaration of Interest.

Acknowledgment

We thank the technical support for confocal microscopy and transmission electron microscope (TEM) at the Core Facility for Integrated Microscopy (CFIM) and that for FACS at the Flow Cytometry & Single Cell Core Facility at the Health and Medical Faculty at the University of Copenhagen. This work was supported by research grants from Nordea-fonden (L.J.R.), Olav Thon Foundation (L.J.R.), Novo Nordisk Foundation NNF17OC0027812 (L.J.R.). L.J.R. is a member of the Clinical Academic Group: Recovery Capacity After Acute Illness in An Aging Population (RECAP). We acknowledge support from the Intramural Program of the National Institute on Aging, National Institutes of Health, USA. Nicotinamide (NR) was obtained from Chromadex Corp., which has a CRADA with Vilhelm Bohr. Support for the metabolomics studies was provided in part by the UCSD Christini Fund and the UCSD Mitochondrial Disease Research Fund.

Appendix A. Supplementary data

Supplementary data to this article can be found online at https://doi.org/10.1016/j.heliyon.2023.e17392.

References

[1] D.B. Lombard, K.F. Chua, R. Mostoslavsky, S. Franco, M. Gostissa, F.W. Alt, DNA repair, genome stability, and aging, Cell 120 (2005) 497–512, https://doi.org/10.1016/j.cell.2005.01.028.

[2] C. Guo, T.-S. Tang, M. Bienko, J.L. Parker, A.B. Bielen, E. Sonoda, S. Takeda, H.D. Ulrich, I. Dikic, E.C. Friedberg, Ubiquitin-binding motifs in REV1 protein are required for its role in the tolerance of DNA damage, Mol. Cell Biol. 26 (2006) 8892–8900, https://doi.org/10.1128/mcb.01118-06.

[3] M.K. Zeman, K.A. Cimprich, Causes and consequences of replication stress, Nat. Cell Biol. 16 (2014) 2–9, https://doi.org/10.1038/ncb2897.

[4] N.B. Fakouri, T.L. Hansen, C. Desler, S. Anugula, L.J. Rasmussen, From powerhouse to perpetrator—mitochondria in health and disease, Biology 8 (2019), https://doi.org/10.3390/biology8020035.

[5] N.B. Fakouri, J.A. Durhuus, C.E. Regnell, M. Angleys, C. Desler, M.M. Hasan-Olive, A. Martín-Pardillos, A. Tsaalbi-Shtylik, K. Thomsen, M. Lauritzen, et al., Rev1 contributes to proper mitochondrial function via the PARP-NAD(+)-SIRT1-PGC1α axis, Sci. Rep. 7 (2017), 12480, https://doi.org/10.1038/s41598-017-12662-3.

[6] A. Martín-Pardillos, A. Tsaalbi-Shtylik, S. Chen, S. Lazare, R.P. van Os, A. Dethmers-Ausema, N.B. Fakouri, M. Bosshard, R. Aprigliano, B. van Loon, et al., Genomic and functional integrity of the hematopoietic system requires tolerance of oxidative DNA lesions, Blood 130 (2017) 1523–1534, https://doi.org/10.1182/blood-2017-01-764274.

[7] N. Sabouri, J. Viberg, D.K. Goyal, E. Johansson, A. Chabes, Evidence for lesion bypass by yeast replicative DNA polymerases during DNA damage, Nucleic Acids Res. 36 (2008) 5660–5667, https://doi.org/10.1093/nar/gkn555.

[8] M.B. Davidson, Y. Katou, A. Keszthelyi, T.L. Sing, T. Xia, J. Ou, J.A. Vaisica, N. Thevakumaran, L. Marjavaara, C.L. Myers, et al., Endogenous DNA replication stress results in expansion of dNTP pools and a mutator phenotype, EMBO J. 31 (2012) 895–907, https://doi.org/10.1038/emboj.2011.485.

[9] J. Poli, O. Tsaponina, L. Crabbé, A. Keszthelyi, V. Pantesco, A. Chabes, A. Lengronne, P. Pasero, dNTP pools determine fork progression and origin usage under replication stress, EMBO J. 31 (2012) 883–894, https://doi.org/10.1038/emboj.2011.470.

[10] P.J. Oliveira, K.B. Wallace, Depletion of adenine nucleotide translocator protein in heart mitochondria from doxorubicin-treated rats–relevance for mitochondrial dysfunction, Toxicology 220 (2006) 160–168, https://doi.org/10.1016/j.tox.2005.12.009.

[11] W. Chen, L. Zhang, K. Zhang, B. Zhou, M.-L. Kuo, S. Hu, L. Chen, M. Tang, Y.-R. Chen, L. Yang, et al., Reciprocal regulation of autophagy and dNTP pools in human cancer cells, Autophagy 10 (2014) 1272–1284, https://doi.org/10.4161/auto.28954.

[12] Rev1 deficiency induces replication stress to cause metabolic dysfunction differently in males and females, in: W. Het Panhuis, A. Tsaalbi-Shtylik, M. Schönke, V. van Harmelen, A.C.M. Pronk, T.C.M. Streefland, H.C.M. Sips, S. Afkir, K. Willems van Dijk, P.C.N. Rensen, et al. (Eds.), Am. J. Physiol. Endocrinol. Metab. 322 (2022) E319–E329, https://doi.org/10.1152/ajpendo.00357.2021.

[13] C. Cantó, K.J. Menzies, J. Auwerx, NAD+ metabolism and the control of energy homeostasis: a balancing act between mitochondria and the nucleus, Cell Metabol. 22 (2015) 31–53, https://doi.org/10.1016/j.cmet.2015.05.023.

[14] Y. Aman, J. Frank, S.H. Lautrup, A. Matysek, Z. Niu, G. Yang, L. Shi, L.H. Bergersen, J. Storm-Mathisen, L.J. Rasmussen, et al., The NAD+-mitophagy axis in healthy longevity and in artificial intelligence-based clinical applications, Mech. Ageing Dev. 185 (2020), 111194, https://doi.org/10.1016/j.mad.2019.111194.

[15] S. Srivastava, Emerging therapeutic roles for NAD(+) metabolism in mitochondrial and age-related disorders, Clin. Transl. Med. 5 (2016) 25, https://doi.org/10.1186/s40169-016-0104-7.

[16] S. ichiro Imai, L. Guarente, NAD+ and sirtuins in aging and disease, Trends Cell Biol. 24 (2014) 464–471, https://doi.org/10.1016/j.tcb.2014.04.002.

[17] E. Verdin, NAD^+ in aging, metabolism, and neurodegeneration, Science 350 (2015) 1208–1213, https://doi.org/10.1126/science.aac4854.

[18] S. Johnson, S.I. Imai, NAD (+) biosynthesis, aging, and disease, F1000Res 7 (2018) 132, https://doi.org/10.12688/f1000research.12120.1.

[19] E.F. Fang, Y. Hou, S. Lautrup, M.B. Jensen, B. Yang, T. SenGupta, D. Caponio, R. Khezri, T.G. Demarest, Y. Aman, et al., NAD(+) augmentation restores mitophagy and limits accelerated aging in Werner syndrome, Nat. Commun. 10 (2019) 5284, https://doi.org/10.1038/s41467-019-13172-8.

[20] E.F. Fang, H. Kassahun, D.L. Croteau, M. Scheibye-Knudsen, K. Marosi, H. Lu, R.A. Shamanna, S. Kalyanasundaram, R.C. Bollineni, M.A. Wilson, et al., NAD(+) replenishment improves lifespan and healthspan in ataxia telangiectasia models via mitophagy and DNA repair, Cell Metabol. 24 (2016) 566–581, https://doi.org/10.1016/j.cmet.2016.09.004.

[21] J. Fan, K.A. Krautkramer, J.L. Feldman, J.M. Denu, Metabolic regulation of histone post-translational modifications, ACS Chem. Biol. 10 (2015) 95–108, https://doi.org/10.1021/cb500846u.

[22] A. Croset, F.P. Cordelières, N. Berthault, C. Buhler, J.S. Sun, M. Quanz, M. Dutreix, Inhibition of DNA damage repair by artificial activation of PARP with siDNA, Nucleic Acids Res. 41 (2013) 7344–7355, https://doi.org/10.1093/nar/gkt522.

[23] C. Cantó, A.A. Sauve, P. Bai, Crosstalk between poly(ADP-ribose) polymerase and sirtuin enzymes, Mol. Aspect. Med. 34 (2013) 1168–1201, https://doi.org/10.1016/j.mam.2013.01.004.

[24] T. Peled, H. Shoham, D. Aschengrau, D. Yackoubov, G. Frei, N. Rosenheimer G, B. Lerrer, H.Y. Cohen, A. Nagler, E. Fibach, et al., Nicotinamide, a SIRT1 inhibitor, inhibits differentiation and facilitates expansion of hematopoietic progenitor cells with enhanced bone marrow homing and engraftment, Exp. Hematol. 40 (2012) 342–355, https://doi.org/10.1016/j.exphem.2011.12.005, e1.

[25] E.F. Fang, M. Scheibye-Knudsen, L.E. Brace, H. Kassahun, T. Sengupta, H. Nilsen, J.R. Mitchell, D.L. Croteau, V.A. Bohr, Defective mitophagy in XPA via PARP-1 hyperactivation and NAD +/SIRT1 reduction, Cell 157 (2014) 882–896, https://doi.org/10.1016/j.cell.2014.03.026.

[26] M. Scheibye-Knudsen, S.J. Mitchell, E.F. Fang, T. Iyama, T. Ward, J. Wang, C.A. Dunn, N. Singh, S. Veith, M.M. Hasan-Olive, et al., A high-fat diet and NAD(+) activate Sirt1 to rescue premature aging in cockayne syndrome, Cell Metabol. 20 (2014) 840–855, https://doi.org/10.1016/j.cmet.2014.10.005.

[27] E. Turunc Bayrakdar, Y. Uyanikgil, L. Kanit, E. Koylu, A. Yalcin, Nicotinamide treatment reduces the levels of oxidative stress, apoptosis, and PARP-1 activity in Aβ(1-42)-induced rat model of Alzheimer's disease, Free Radic. Res. 48 (2014) 146–158, https://doi.org/10.3109/10715762.2013.857018.

[28] Y.J. Hou, S. Lautrup, S. Cordonnier, Y. Wang, D.L. Croteau, E. Zavala, Y.Q. Zhang, K. Moritoh, J.F. O'Connell, B.A. Baptiste, et al., NAD(+) Suppl. Norm. key Alzheimer's Featur. DNA damage responses a new AD mouse Model with Introd, DNA repair Defic 115 (2018) E1876–E1885.

[29] E.F. Fang, H. Kassahun, D.L. Croteau, M. Scheibye-Knudsen, K. Marosi, H.M. Lu, R.A. Shamanna, S. Kalyanasundaram, R.C. Bollineni, M.A. Wilson, et al., NAD(+) replenishment improv. Lifesp. heal. Ataxia telangiectasia model, via Mitophagy DNA Repair 24 (2016) 566–581.

[30] S. Martire, L. Mosca, M. d'Erme, PARP-1 involvement in neurodegeneration: a focus on Alzheimer's and Parkinson's diseases, Mech. Ageing Dev. 146 (2015) 53–64, https://doi.org/10.1016/j.mad.2015.04.001, 148.

[31] M.S. Jurkowitz, M.L. Litsky, M.J. Browning, C.M. Hohl, Adenosine, inosine, and guanosine protect glial cells during glucose deprivation and mitochondrial inhibition: correlation between protection and ATP preservation, J. Neurochem. 71 (1998) 535–548, https://doi.org/10.1046/j.1471-4159.1998.71020535.x.

[32] B. Ullman, L.J. Gudas, A. Cohen, D.W.J. Martin, Deoxyadenosine metabolism and cytotoxicity in cultured mouse T lymphoma cells: a model for immunodeficiency disease, Cell 14 (1978) 365–375, https://doi.org/10.1016/0092-8674(78)90122-8.

[33] V. Fridman, S. Zarini, S. Sillau, K. Harrison, B.C. Bergman, E.L. Feldman, J.E.B. Reusch, B.C. Callaghan, Altered plasma serine and 1-deoxydihydroceramide profiles are associated with diabetic neuropathy in type 2 diabetes and obesity, J. Diabet. Complicat. 35 (2021), 107852, https://doi.org/10.1016/j.jdiacomp.2021.107852.

[34] S.M. Hammad, N.L. Baker, J.M. El Abiad, S.D. Spassieva, J.S. Pierce, B. Rembiesa, J. Bielawski, M.F. Lopes-Virella, R.L. Klein, Increased plasma levels of select deoxy-ceramide and ceramide species are associated with increased odds of diabetic neuropathy in type 1 diabetes: a pilot study, NeuroMolecular Med. 19 (2017) 46–56, https://doi.org/10.1007/s12017-016-8423-9.

[35] H. Nakayama, M. Nagafuku, A. Suzuki, K. Iwabuchi, J.-I. Inokuchi, The regulatory roles of glycosphingolipid-enriched lipid rafts in immune systems, FEBS Lett. 592 (2018) 3921–3942, https://doi.org/10.1002/1873-3468.13275.

[36] A.M. Miranda, Z.M. Lasiecka, Y. Xu, J. Neufeld, S. Shahriar, S. Simoes, R.B. Chan, T.G. Oliveira, S.A. Small, G. Di Paolo, Neuronal lysosomal dysfunction releases exosomes harboring APP C-terminal fragments and unique lipid signatures, Nat. Commun. 9 (2018) 291, https://doi.org/10.1038/s41467-017-02533-w.

[37] K.C. Patra, N. Hay, The pentose phosphate pathway and cancer, Trends Biochem. Sci. 39 (2014) 347–354, https://doi.org/10.1016/j.tibs.2014.06.005.

[38] E.F. Fang, Y. Hou, S. Lautrup, M.B. Jensen, B. Yang, T. SenGupta, D. Caponio, R. Khezri, T.G. Demarest, Y. Aman, et al., NAD(+) Augment. restores mitophagy limits Accel, aging Werner Syndr 10 (2019) 5284.

[39] J.N.S. Vargas, C. Wang, E. Bunker, L. Hao, D. Maric, G. Schiavo, F. Randow, R.J. Youle, Spatiotemporal control of ULK1 activation by NDP52 and TBK1 during selective autophagy, Mol. Cell 74 (2019) 347–362, https://doi.org/10.1016/j.molcel.2019.02.010, e6.

[40] S.A. Detmer, D.C. Chan, Functions and dysfunctions of mitochondrial dynamics, Nat. Rev. Mol. Cell Biol. 8 (2007) 870–879, https://doi.org/10.1038/nrm2275.

[41] I. van Bostelen, M. Tijsterman, Combined loss of three DNA damage response pathways renders C. elegans intolerant to light, DNA Repair 54 (2017) 55–62, https://doi.org/10.1016/j.dnarep.2017.04.002.

[42] I. van Bostelen, R. van Schendel, R. Romeijn, M. Tijsterman, Translesion synthesis polymerases are dispensable for C. elegans reproduction but suppress genome scarring by polymerase theta-mediated end joining, PLoS Genet. 16 (2020), e1008759, https://doi.org/10.1371/journal.pgen.1008759.

[43] B.C. Gilmour, R. Gudmundsrud, J. Frank, A. Hov, S. Lautrup, Y. Aman, H. Rosjo, C. Brenner, M. Ziegler, O.B. Tysnes, et al., Target. NAD(+) transl. Res. To reli. Dis. Cond. Metab. Stress ageing, Mech. Ageing Dev. 186 (2020).
[44] G.A. Patwardhan, L.J. Beverly, L.J. Siskind, Sphingolipids and mitochondrial apoptosis, J. Bioenerg. Biomembr. 48 (2016) 153–168, https://doi.org/10.1007/s10863-015-9602-3.
[45] M. Maceyka, S. Spiegel, Sphingolipid metabolites in inflammatory disease, Nature 510 (2014) 58–67, https://doi.org/10.1038/nature13475.
[46] P.J. Meikle, S.A. Summers, Sphingolipids and phospholipids in insulin resistance and related metabolic disorders, Nat. Rev. Endocrinol. 13 (2017) 79–91, https://doi.org/10.1038/nrendo.2016.169.
[47] S. Miyamoto, C.-C. Hsu, G. Hamm, M. Darshi, M. Diamond-Stanic, A.-E. Declèves, L. Slater, S. Pennathur, J. Stauber, P.C. Dorrestein, et al., Mass spectrometry imaging reveals elevated glomerular ATP/AMP in diabetes/obesity and identifies sphingomyelin as a possible mediator, EBioMedicine 7 (2016) 121–134, https://doi.org/10.1016/j.ebiom.2016.03.033.
[48] C. Cantó, Z. Gerhart-Hines, J.N. Feige, M. Lagouge, L. Noriega, J.C. Milne, P.J. Elliott, P. Puigserver, J. Auwerx, AMPK regulates energy expenditure by modulating NAD + metabolism and SIRT1 activity, Nature 458 (2009) 1056–1060, https://doi.org/10.1038/nature07813.
[49] J.G. Jansen, P. Langerak, A. Tsaalbi-Shtylik, P. van den Berk, H. Jacobs, N. de Wind, Strand-biased defect in C/G transversions in hypermutating immunoglobulin genes in Rev1-deficient mice, J. Exp. Med. 203 (2006) 319–323, https://doi.org/10.1084/jem.20052227.
[50] K. Li, J.C. Naviaux, A.T. Bright, L. Wang, R.K. Naviaux, A robust, single-injection method for targeted, broad-spectrum plasma metabolomics, Metabolomics 13 (2017) 122, https://doi.org/10.1007/s11306-017-1264-1.
[51] J.-H. Um, Y.Y. Kim, T. Finkel, J. Yun, Sensitive measurement of mitophagy by flow cytometry using the pH-dependent fluorescent reporter mt-keima, J. Vis. Exp. (2018), https://doi.org/10.3791/58099.